Magnonic contribution in thermal conductance of a nanostructure in the presence of magnon-phonon interaction

Sahar Shojaei,[1,*] Mohammad Mardaani,[1,2,†] and Hassan Rabani[1,2,‡]
[1]*Department of Physics, Faculty of Science, Shahrekord University, P.O. Box 115, Shahrekord, Iran*
[2]*Nanotechnology Research Center, Shahrekord University, 8818634141, Shahrekord, Iran*

(Received 5 April 2022; accepted 27 July 2022; published 22 August 2022)

Using Green's function method, we study thermal transport properties of magnons transmitting through a magnetic nanowire at a certain temperature. In a small part of the nanowire in the middle, we are supposed to have two types of local and nonlocal magnon-phonon interactions. The self-energies for this part due to the other parts of the wire are analytically derived. First, we calculate the phonon mode-dependent magnon transmission coefficient in the classical canonical ensemble. Then, by taking an average of the phonon modes, we obtain the total magnon transmission coefficient and use it for computing magnon thermal conductance. We use the model to investigate four configurations of magnetic nanowires composed of ferromagnetic and/or antiferromagnetic parts. The results show that, when the scattering region has an antiferromagnetic alignment, the magnons transfer in the structure more weakly than for ferromagnetic alignment. There is a phonon-assisted mechanism for tunneling of magnons which are transmitted through the gap or between magnon quasifrequencies of the scattering region. Generally, in the same values for local and nonlocal strengths of magnon-phonon interaction, the nonlocal one has a greater effect on the magnonic thermal transport properties. We found the fitting functions in order to relate the macroscopic quantities of the magnon transmission coefficient and thermal conductivity to microscopic parameters of the strengths of the local and nonlocal magnon-phonon interaction.

DOI: 10.1103/PhysRevE.106.024122

I. INTRODUCTION

In the last decade, technological advances, especially in the fields of quantum computation and spintronics, have been accomplished by the use of the electron and its spin [1,2]. The study of low-dimensional quantum ferromagnets and antiferromagnets [3,4], the coherent scattering of elementary spin excitations or magnons [5], and the importance of magnetic anisotropy [6] in nanostructures have attracted great interest from theoretical and experimental scientists because of their strange physical properties [7]. The plurality of these related research activities has been directed toward the reach of quantum transmission in low-dimensional magnetic systems including one-dimensional (1D) spin chains [8–10], spin ladders [11], two-dimensional (2D) quantum magnets [12–14], and quasi-2D-layered van der Waals materials [15]. An important class of materials that host such quantum magnets is formed by copper oxides [16], for instance $SrCuO_2$ [17] in 1D and La_2CuO_4 [18] in 2D magnetic systems. The strength of the interaction between magnetic moments or exchange coupling in these materials depends on their structures. As mentioned, the important advantage of utilizing magnons is that they transport information and heat in classical spin waves. The quanta of this spin-wave energy are $\hbar\omega$ and its frequency, ω, can reach the terahertz range [19,20]. To obtain the energy transport in Heisenberg chains, inelastic neutron scattering as an experimental method is available [21]. Thermal transport by phonons and electrons has been comprehensively studied [22,23]. The magnetothermal conductivity in magnetic systems was initially predicted by H. Frohlich in 1936 [24], but it took several years to be experimentally affirmed and become established as a novel contribution to total thermal conductivity [25,26]. Most of the experiments were interesting for revealing the spin Hall [27] and spin Seebeck effects [28] and the Wiedemann-Franz law [29]. Development of fascinating applications of insulating materials with large thermal conductance due to magnetic excitations [30], the interaction of spinons with structural defects, electrons, and quasiparticles such as phonons [31–34] and magnons [35,36] demonstrates intriguing features in spintronic-based systems [37,38]. For example, recent research has demonstrated that electron-magnon interaction in high fields can cause a decrease in the high-field resistivity of ferromagnetic materials [39].

Theoretical calculations of the 1D Heisenberg model were highlighted as a key to realizing thermal transport in ferromagnet- and antiferromagnet-based magnon devices [40,41]. The main focus of this paper has been on computing the magnon transmission coefficient and thermal conductance for an extended magnetic chain using Green's function technique. Some magnetic moments in the middle of the chain are assumed to be vibrating, and the consideration of magnon-phonon interaction will be interesting. We perform our calculations in the presence of a dissipative environment at a certain temperature.

*saharshojaie75@gmail.com
†mohammad-m@sku.ac.ir
‡rabani-h@sku.ac.ir

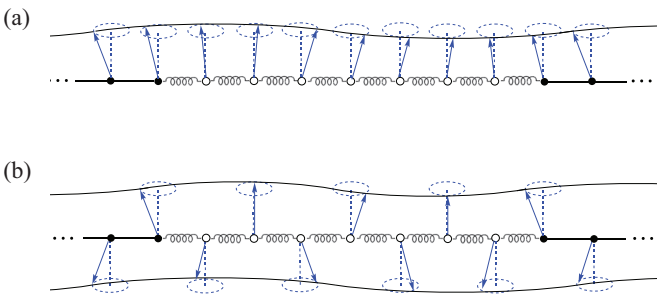

FIG. 1. Schematic picture of magnon propagating (solid wavy line) in (a) ferromagnetic and (b) antiferromagnetic chains. The magnetic moments are represented by vectors and their precession in the *xy* plane is shown by dotted circles. In the middle of the chain, the moments, which are displayed by empty bullets, can vibrate via springs, leading to the magnon-phonon interaction. The filled bullets, which are connected by solid lines, are used for the sites in the nonvibrating leads.

The scheme of the paper is as follows. With this brief introduction (Sec. I), in Sec. II, we describe the model and theoretical framework. In Sec. III, we discuss the numerical results for some examples. Finally, we conclude our study in Sec. IV.

II. MODEL AND FORMALISM

Consider the magnon transfer through a nanowire including N vibrating magnetic moments, which are connected to two semi-infinite similar rigid magnetic leads via two rigid contacts. The leads and the wire are supposed to have ferromagnetic (F) or antiferromagnetic (A) alignments. For example, Figs. 1(a) and 1(b) display the schematic pictures corresponding to FFF and AAA configurations, respectively. We label the magnetic moment sites with integer p so that the ranges of $[-\infty,\ldots,0]$, $[1,\ldots,N]$, and $[N+1,\ldots,\infty]$ for p respectively distinguish the sites on the left lead (L), center wire (W), and right lead (R). The pth dimensionless magnetic moment obeys the following Bloch-type equation [42]:

$$\frac{d\vec{S}_p}{dt}+\frac{\vec{S}_p}{\tau_p}=\frac{J_{p-1}}{\hbar}\vec{S}_p\times\vec{S}_{p-1}+\frac{J_{p+1}}{\hbar}\vec{S}_p\times\vec{S}_{p+1}, \tag{1}$$

where $J_{p\pm1}$ is the exchange integral between p and $p\pm1$ moments and $\tau_p=\gamma_p^{-1}$ is the magnon relaxation time. We set $\vec{S}_p=[S_{p,x},S_{p,y},(-1)^{\delta(p+1)}]$ in which $|S_{p,x}|$ and $|S_{p,y}|$ are significantly smaller than one [42–44]. Here, in the third coordinate, δ takes the values zero and one for ferromagnetic and antiferromagnetic alignments, respectively. To explain it further, the definition of normal collective modes such as magnon in ferromagnetic and antiferromagnetic materials originated from the superposition principle that means the governed wave equation on the magnetic behavior of the system should be linear. By definition of $S_p^+=S_{p,x}+iS_{p,y}=\tilde{S}_p^+e^{-i\omega t}$, where $\tilde{S}_p$ and ω are amplitude and frequency of the propagating magnon, we have

$$[(-1)^{\delta(p+1)}(\hbar\omega+i\hbar\gamma_p)+(-1)^{\delta+1}(J_{p-1}+J_{p+1})]\tilde{S}_p^+ +J_{p-1}\tilde{S}_{p-1}^+ +J_{p+1}\tilde{S}_{p+1}^+=0. \tag{2}$$

From the above equation, working with Dirac notation, we can arrive directly at the following definition for Green's function matrix of isolated center wire, $\mathbf{G}_0^{(n)}$, as follows:

$$\frac{1}{\mathbf{G}_0^{(n)}}=\sum_{p=1}^{N}f_p|\tilde{S}_p^+\rangle\langle\tilde{S}_p^+|+\sum_{p=1}^{N-1}J_{p+1}|\tilde{S}_p^+\rangle\langle\tilde{S}_{p+1}^+| +\sum_{p=2}^{N+1}J_{p-1}|\tilde{S}_p^+\rangle\langle\tilde{S}_{p-1}^+|+\text{H.c.}, \tag{3}$$

where

$$f_p=(-1)^{\delta(p+1)}(\hbar\omega+i\hbar\gamma_p)+(-1)^{\delta+1}(J_{p-1}+J_{p+1}).$$

H.c. is the Hermitian conjugate of two previous sums and n refers to the phonon because the magnon-phonon interaction is present. Since the moments in the center wire are assumed to be vibrating, the phonons play an important role in transferring magnons due to the phonon-magnon interaction. The scenario in which the exchange integral varies by the distance between charge distributions is described by some authors [45–47]. Here, we explain the origin of this content by the following bielectronic exchange integral for the neighboring moments [48]:

$$J_{p,p\pm1}=\frac{1}{4\pi\varepsilon_0}\int\phi_p^*(\mathbf{r}_1)\phi_{p\pm1}^*(\mathbf{r}_2) \times\frac{-e^2}{|\mathbf{r}_1-\mathbf{r}_2|}\phi_{p\pm1}(\mathbf{r}_1)\phi_p(\mathbf{r}_2)d\mathbf{r}_1d\mathbf{r}_2,$$

where $\phi_p^*(\mathbf{r})\phi_{p\pm1}(\mathbf{r})$ is charge distribution, $\mathbf{r}_1=\mathbf{r}_p-u_p\hat{x}$, and $\mathbf{r}_2=\mathbf{r}_{p\pm1}-(a+u_{p\pm1})\hat{x}$, in which u_p is the displacement from the equilibrium position of the pth moment. Here, $\mathbf{r}_p$ represents the electron positions in the pth site of the chain and a is the lattice constant. One can expand the above exchange energy as

$$J_{p\pm1}=J_W+\frac{\partial J_{p,p\pm1}}{\partial X_p}\Big|_{X_p=a}(u_{p\pm1}-u_p), \tag{4}$$

where $X_p=a+u_{p\pm1}-u_p$ is the relative displacement variable. Therefore, the exchange integrals in terms of dimensionless phonon-mode (n) dependent moment displacements can be written as follows:

$$J_{p\pm1}=J_W\big[1+\lambda\big(\tilde{u}_p^{(n)}-\tilde{u}_{p\pm1}^{(n)}\big)\big], \tag{5}$$

where J_W is the exchange integral between moments in the absence of vibration. Its typical value is on the order of 0.01 eV [49]. Also, λ is the strength of the nonlocal magnon-phonon interaction and compared with Eq. (4) reads $\lambda=-a(\partial J_{p\pm1}/\partial X_p)_{X_p=a}/J_W$. Consequently, we separate the frequency dependence of the magnon-phonon interaction in the exchange integral as well as admit the λ remains the only amplitude of this interaction. In Eq. (5), $\tilde{u}_p^{(n)}$ is the dimensionless displacement from the equilibrium position of a pth moment at the nth phonon mode [50,51],

$$\tilde{u}_p^{(n)}=\xi\frac{\sqrt{2}}{\sqrt{N+1}}\sin\frac{np\pi}{N+1}, \tag{6}$$

where ξ is a dimensionless variable for displacements in the center wire. Moreover, it is also a temperature-dependent parameter, and by the help of the equipartition theorem we have

$\langle \xi^2 \rangle = k_B T / m\omega_n^2 a^2$, in which m is the mass of each moment and ω_n is the phonon frequency of mode n. By substituting Eq. (6) into Eq. (5), we found that $J_{p\pm1}$ is explicitly temperature dependent (via ξ parameter) and mode dependent (via n). When the vibration amplitudes increase by increasing the temperature, then the magnon-phonon interaction increases. In the following, we suppose that the dissipative magnon energy is proportional to the vibrating kinetic energy of the moments. Indeed, we suppose that the magnon passing from a local atom will be scattered by ion vibration. More atomic vibrations lead to increased magnon scattering. We quantify this event as follows: Whenever the kinetic energy of the located atom rises, the magnon scatters more [$\hbar\gamma_p \propto m(v_p^{ion})^2$ in which v_p^{ion} is the velocity of the pth atom] and it behaves like a dissipative environment for the magnon. In another way [52], γ_p is proportional to $k_B T$, which demonstrates that our assumption is credible and plausible physically. Therefore, we have

$$\gamma_p = \frac{\gamma \omega_0^{\mathrm{ph}}}{N+1}\left(\xi_{\max}^2 - \xi^2\right)\sin^2\frac{np\pi}{N+1}\sin^2\frac{n\pi}{2(N+1)}, \tag{7}$$

where γ is the magnon damping coefficient or the strength of the local magnon-phonon interaction, $\xi_{\max}$ is the maximum value of ξ, and $\omega_0^{\mathrm{ph}} = \sqrt{2C/m}$ in which C is the force constant between the moments in the center wire. When the center wire is connected to the magnetic leads, its Green's function matrix for the nth phonon mode is rewritten as

$$\mathbf{G}_W^{(n)} = \frac{\mathbf{G}_0^{(n)}}{1 - \mathbf{G}_0^{(n)}(\mathbf{\Sigma}_L + \mathbf{\Sigma}_R)}, \tag{8}$$

where $\mathbf{\Sigma}_{L(R)}$ is the self-energy matrix due to the existence of left (right) lead of which its elements read

$$(\mathbf{\Sigma}_{L(R)})_{p,q} = \Sigma_{L(R)}\delta_{p,1(N)}, \tag{9a}$$

where for ferromagnets

$$\Sigma_{L(R)} = \frac{J_{WL(R)}^2}{2J_{L(R)}^2}\left(2J_{L(R)} - \hbar\omega - \sqrt{\hbar^2\omega^2 - 4\hbar\omega J_{L(R)}}\right), \tag{9b}$$

and for antiferromagnets

$$\Sigma_{L(R)} = \frac{J_{WL(R)}^2[4J_{L(R)} + 2\hbar\omega(\zeta_{L(R)})^N]}{4J_{L(R)}^2 - \hbar^2\omega^2 + \hbar\omega\sqrt{\hbar^2\omega^2 - 4J_{L(R)}^2}}, \tag{9c}$$

where $\zeta_L = 1$ and $\zeta_R = -1$. The above functions are obtained by using Eq. (2) for a semi-infinite ideal lead with the help of surface Green's function matrices and dispersion relations for ferromagnetic and antiferromagnetic chains [53]. Their derivations are similar to the electronic ones in the tight-binding approach. For ferromagnetic and antiferromagnetic cases they correspond to simple and alternating on-site/hopping chains. Using the formulas in Ref. [50], for the ferromagnetic case, we substitute on-site energy by $2J_{L(R)}$ and the hopping by $-J_{L(R)}$. Correspondingly, for the antiferromagnetic case in self-energy formulas in Refs. [54,55], we substitute alternating on-site energies by $2J_{L(R)}$ and $-2J_{L(R)}$ and the alternating hoppings by $J_{L(R)}$ and $-J_{L(R)}$. Now, we can calculate the mode dependence of the magnon transmission coefficient by

$$T_n(\omega, \xi) = 4\,\mathrm{Im}\,\Sigma_L\,\mathrm{Im}\,\Sigma_R\left|\left(\mathbf{G}_W^{(n)}\right)_{1,N}\right|^2. \tag{10}$$

To use the above relation, for ferromagnetic and antiferromagnetic leads, one should choose $\Sigma_{L(R)}$ in Eqs. (9b) and (9c), respectively. Also, $(\mathbf{G}_W^{(n)})_{1,N}$ must be written for the corresponding structure that is located between leads. For example, for FAF configuration, both Σ_L and Σ_R are from Eq. (9b), and for $(\mathbf{G}_0^{(n)})_{1,N}$ in Eq. (8), which is given by Eq. (3), δ is zero. The following thermal average in the canonical ensemble eliminates the phonon degrees of freedom, leading to

$$\langle T_n(\omega)\rangle = \frac{1}{Z_n}\int_{-\xi_c}^{\xi_c} T_n(\omega, \xi)\exp\left(-\beta m\omega_n^2 a^2\xi^2/2\right)d\xi, \tag{11}$$

where ξ_c is the cutoff of ξ that usually takes the value of 0.4 (see, e.g., Lindemann criterion of melting [48]), $\omega_n = \omega_0^{\mathrm{ph}}|\sin n\pi/2(N+1)|$, and a is the lattice constant. Moreover, Z_n is the partition function that is

$$Z_n = \int_{-\xi_c}^{\xi_c}\exp\left(-\beta m\omega_n^2 a^2\xi^2/2\right)d\xi. \tag{12}$$

Finally, the total magnon transmission coefficient is obtained by the following average:

$$T_{tot} = \frac{1}{N}\sum_{n=1}^{N}\langle T_n(\omega)\rangle. \tag{13}$$

Also, the magnon thermal conductance can be calculated by

$$\kappa = \frac{k_B\beta^2\hbar^2}{2\pi}\int_0^{\omega_{\max}} T_{tot}(\omega)\frac{\omega^2 e^{\beta\hbar\omega}}{(e^{\beta\hbar\omega}-1)^2}d\omega. \tag{14}$$

The quasi-one-dimensional density of states is used in the above relation. In the next section, we apply our model for the magnetic chains with FFF, AAA, FAF, and AFA configurations to compute and compare their magnonic transport properties.

III. RESULTS

Here, we present the results of our calculation regarding the magnonic transport properties of some infinite magnetic chains with FFF, AAA, FAF, and AFA configurations in which the magnon-phonon interaction exists only on a small part of them, which is called the center part. The other parts, which are named left and right leads, are assumed to be similar and ideal, without any interaction. We investigate how the magnon transmission coefficient and thermal conductance can be influenced by magnon-phonon interaction. Considering that $\lambda = -a(\partial J_{p\pm1}/\partial X_p)_{X_p=a}/J_W$, when $J_{p\pm1}$ is a rapidly descending function like $J \approx J_W\exp(-X_p/a)$ for the electron in s-wave orbitals, λ takes the value of 1. As a result, we expect that values of 0–1 for λ at least have a correct order and may lie in a realistic scenario. During our calculations, we set $J_W = J_L = J_R = J_0$ and, for the sake of observing confinement effects, we fix the values of $J_{WL(R)}$ at $0.8J_0$. To avoid complexity and achieve better physical conceptions, in most figures, we choose the typical number of ten for the number of magnetic moments in the center wire, N. Moreover, we perform the calculations for the case in which $J_0 = \hbar\omega_0^{\mathrm{ph}}$. Finally, since the phonons are excited at higher temperatures, we prepare the plots for $T = T_0 = J_0/k_B$, which exhibits partly high temperature (T_0 is nearly 120 K for $J_0 \approx 0.01$ eV).

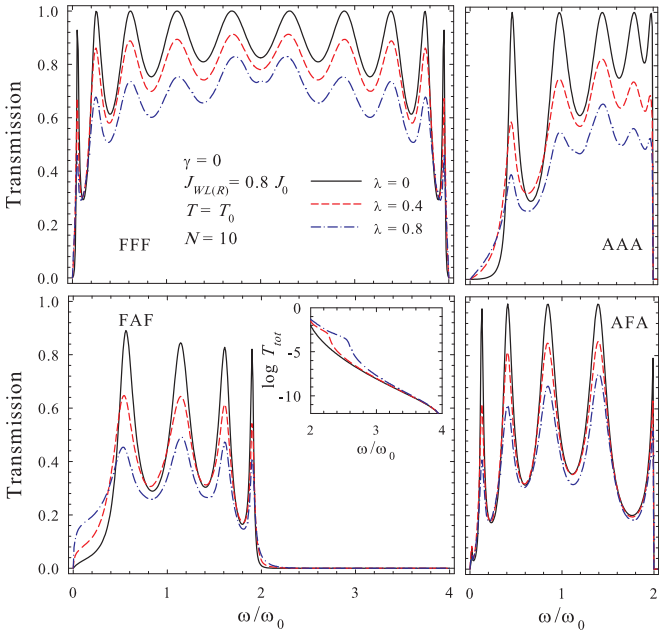

FIG. 2. Magnon transmission coefficient as a function of frequency for a ferromagnetic chain that is connected to two ferromagnetic leads (FFF), an antiferromagnetic chain that is connected to two antiferromagnetic leads (AAA), an antiferromagnetic chain connected to two ferromagnetic leads (FAF), and a ferromagnetic chain connected to two antiferromagnetic leads (AFA). The curves are plotted for high temperatures ($T = T_0$) and for different values of the strength of nonlocal magnon-phonon interaction λ. The numerical values of needed parameters are chosen as follows: $N = 10$, $J_{WL(R)} = 0.8J_0$, $J_{L(R,W)} = J_0$, and $\gamma = 0$. The inset in the FAF plot shows the logarithm of transmission coefficient in the tunneling region: [2,4]ω_0.

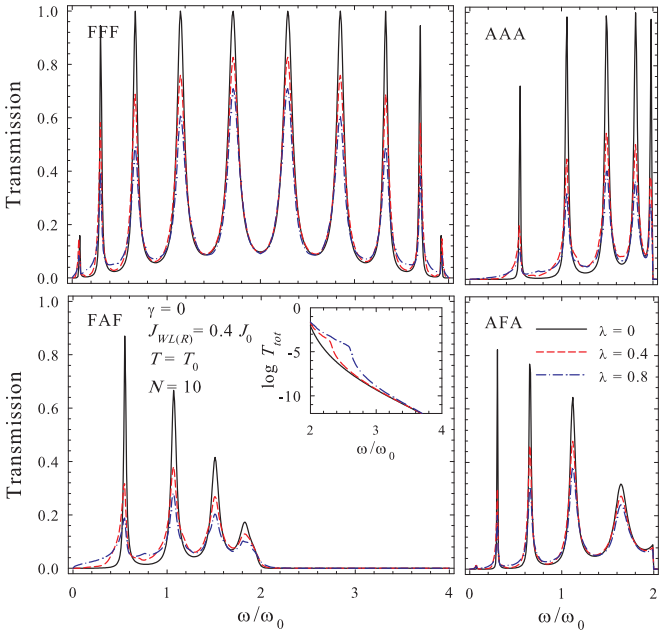

FIG. 3. The same as Fig. 2 except that here $J_{WL(R)} = 0.4J_0$.

In Fig. 2, we plot the magnon transmission coefficients of the mentioned configurations as functions of incoming magnon frequency for different values of strength of nanolocal magnon-phonon interaction in the absence of a local one. The range of magnon frequencies for FFF and FAF configurations is [0,4ω_0], while for AAA and AFA it is [0,2ω_0]. In fact, the allowed frequency windows are determined by magnon band frequencies of leads, which are $\omega = 4\omega_0 \sin^2(ka/2)$ and $\omega = 2\omega_0|\sin(ka/2)|$ for ferromagnetic and antiferromagnetic leads, respectively. Here, k is the magnon wave number and a is the lattice constant. Generally, around the resonance peaks, the magnon conductance decreases by increasing λ. In the tunneling regions and low frequencies (see the plots for the FAF and AAA cases), the magnons transmit better through the system for larger values of λ. This may refer to the phonon-assisted tunneling effect which implies that the phonons help the magnons to tunnel through the magnonic gap or outside of the center wire magnonic band. In the FAF case, for the tunneling region [2ω_0, 4ω_0], we present the logarithm of magnon transmission coefficient at high frequencies in the inset of Fig. 2. We redrew the plots of Fig. 2 for $J_{WL(R)} = 0.4J_0$ in Fig. 3 and found an interesting result. The transmission in the regions between the peaks behaves like that in the tunneling regions, namely, the behavior increases with increasing λ. In fact, in these regions, the overlapping of neighboring magnon quasilevels is reduced and they behave like quasifrequency gaps in which the magnon tunnels. Therefore, the phonon-assisted effect will occur.

Two plots in Fig. 4 display the logarithm of the magnon transmission coefficient of FAF structure versus frequency for two different cases: One in a fixed λ for some small values of N and the other for the fixed N in some different values of λ. The tunneling transmission in the range of [2ω_0, 4ω_0] exponentially decreases by increasing the length of the center chain. When the length of the center chain is fixed, corresponding to the previous figure, the phonon-assisted effect is notable in higher values of λ.

In Fig. 5, the magnon transmission coefficients of FFF, FAF, AAA, and AFA configurations are presented as functions of magnon frequency for different values of magnon damping coefficient at temperature T_0 in the absence of nonlocal magnon-phonon interaction. The number of moments in the region in which the damping is presented is chosen as ten. The magnon conductance of the systems with ferromagnetic leads (FFF and FAF) is more affected by magnon damping with respect to the systems including antiferromagnetic leads (AAA and AFA). Generally, in all cases, the magnon transmission coefficient decreases exponentially by increasing γ in resonance peaks while being independent of the value of γ in the tunneling regions.

In order to give a general overview, here we fit a function for $T(\lambda, \gamma)$ at a fixed frequency corresponding to a peak in the middle of the system conductance spectra, which reads

$$T(\lambda, \gamma) \approx T_{\max} e^{-b\gamma}\left(1 - \frac{c\lambda^n}{\lambda_c^n + \lambda^n}\right), \tag{15}$$

where $T_{\max}$ is the maximum value of T at the selected peak. Also, b, λ_c, and n are fitting parameters whose values depend on the system configuration and are tabulated in Table I. The values of b show that in uniform FFF and AAA configurations, the local magnon-phonon interaction (γ) has less effect on magnon conductance concerning the uniform FAF and AFA

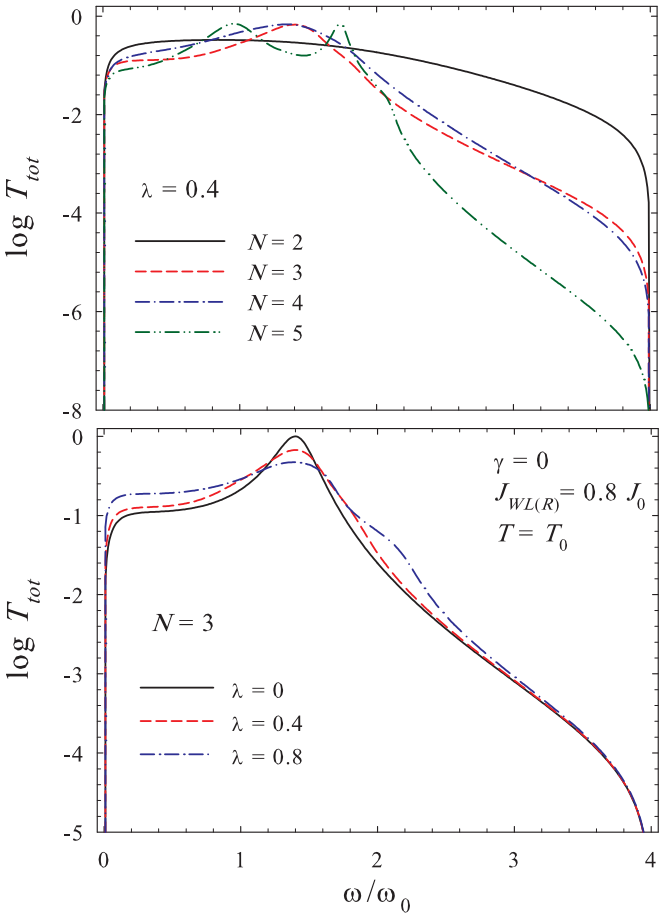

FIG. 4. The logarithm of magnon transmission coefficient as a function of frequency for an antiferromagnetic chain connected to two ferromagnetic leads (FAF) for two cases: One in fixed $\lambda = 0.4$ for different values of N and the other for fixed $N = 3$ in different values of λ. Here, we set $J_{WL(R)} = 0.8J_0$, $J_{L(R,W)} = J_0$, and $\gamma = 0$.

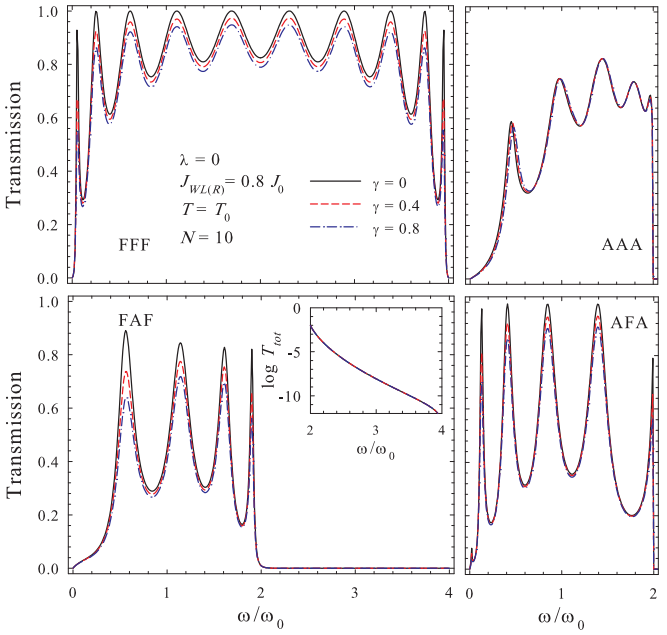

FIG. 5. Magnon transmission coefficient as a function of frequency for the systems of FFF, AAA, FAF, and AFA, at different values of γ in the absence of nonlocal magnon-phonon interaction ($\lambda = 0$). The numerical values of parameters are chosen as follows: $N = 10$, $J_{WL(R)} = 0.8J_0$, $J_{L(R,W)} = J_0$, and $T = T_0$.

configurations. According to the obtained data for c, λ_c, and n, the influence of nonlocal magnon-phonon interaction (λ) becomes weaker, respectively, on FFF, FAF, AFA, and AAA. The small obtained values for b indicate that with compression of γ, λ makes a decrease in T. The last point from Table I is that the values of n depend only on the configuration of leads. The magnon thermal conductances of FFF, AAA, FAF, and AFA configurations versus temperature are shown in Fig. 6 for several different values of λ when the γ is set to zero. Here, κ_0 is a constant with a value of $k_B J_0/(2\pi\hbar)$. Generally, this figure demonstrates that the increase in temperature causes better thermal conductance in all configurations. Also, as expected due to the low phonon excitations, the magnon-phonon interaction has no significant influence at low temperatures. Remarkably, at higher temperatures in the uniform systems of FFF and AAA compared with nonuniform FAF and AFA systems, the magnon thermal conductance is more affected by increasing λ. We find the following fitted function for $\kappa(\lambda, \gamma)$ at the fixed temperature of $T = T_0$:

$$\kappa(\lambda, \gamma) \approx \kappa_{\max} e^{-b\gamma}\left(1 - \frac{c\lambda^n}{\lambda_c^n + \lambda^n}\right), \qquad (16)$$

where $\kappa_{\max}$ is the maximum value of κ at $T = T_0$. Also, b, λ_c, and n are fitting parameters which are tabulated in Table II. This table shows that in the absence of nonlocal magnon-phonon interaction, when the center part has antiferromagnetic alignment, the magnon conductance is more affected by γ. In the absence of local interaction, the magnon thermal conductance in the AAA configuration is more destroyed by λ. In this situation, for small values of λ, Eq. (16) reduces to $\kappa = \kappa_{\max} \exp(-b\gamma - c\lambda^n/{\lambda_c}^n)$. This means that according to Table II the magnon thermal conductance in AAA, AFA, FFF, and FAF, respectively, decrease more with increasing λ. When γ is zero one can find $\lambda = \lambda_c[\ln(\kappa_{\max}/\kappa)/c]^{1/n}$, which gives the strength of nonlocal magnon-phonon interaction in terms of measured magnon thermal conductance. In this way, the microscopic parameter may be understood by proper measurements of magnon thermal conductance in the mentioned systems. n is an important fitting parameter to determine the behavior of κ. Since,

TABLE I. The fitting parameters for $T(\lambda, \gamma)$ in Eq. (15) at a fixed frequency, which is distinguished at the parentheses in the first column, presented for FFF, AAA, FAF, and AFA configurations. In calculation, the following numerical values are chosen for the needed parameters: $T = T_0$, $N = 10$, $J_{WL(R)} = 0.8J_0$, and $J_{L(R,W)} = J_0$.

No.	ω/ω_0	b	c	λ_c	n
FFF	2.9	0.077	0.50	0.82	1.85
FAF	1.14	0.12	0.63	0.83	1.65
AFA	0.97	0.21	0.74	0.65	1.54
AAA	0.85	0.013	0.80	0.67	1.54

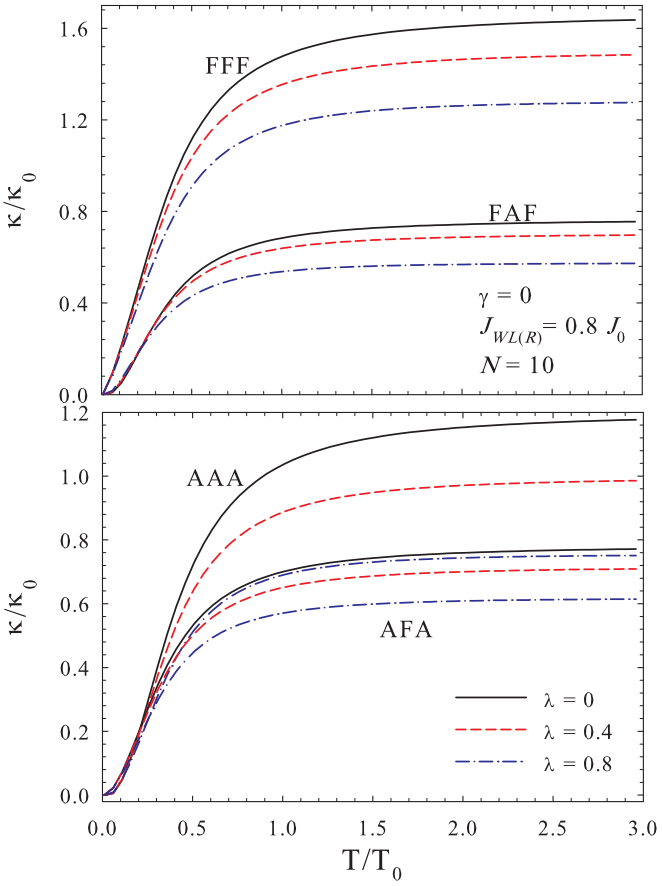

FIG. 6. Magnon thermal conductances of FFF, AAA, FAF, and AFA versus temperature for different values of λ in the absence of local magnon dissipative coefficient ($\gamma = 0$). The numerical values of parameters are chosen as follows: $N = 10$, $J_{WL(R)} = 0.8J_0$, and $J_{L(R,W)} = J_0$.

according to Table II, its value depends on the system configuration, we can conclude that type of structure, dimensionality, and interaction range play a major role in distinguishing the value of n. Next, we plotted in Fig. 7 the magnon thermal conductance as a function of the number of magnetic moments in the central part of the chain. Here, we take $\lambda = 0.4$, $\gamma = 0$, and $T = T_0$. This figure demonstrates that the magnon thermal conductance has the most variation when the number of moments in the center part changes from two to ten. Here, the number of ten distinguishes the length of the center wire corresponding to the magnon wavelength. Since the effective mass of magnons (m^*) in ferromagnetic and antiferromagnetic

TABLE II. The fitting parameters for $\kappa(\lambda, \gamma)$ in Eq. (16) at the fixed temperature of $T = T_0$ for configurations of FFF, AAA, FAF, and AFA. The following numerical values are used in calculations: $N = 10$, $J_{WL(R)} = 0.8J_0$, and $J_{L(R,W)} = J_0$.

No.	b	c	λ_c	n
FFF	0.09	0.59	1.15	1.68
FAF	0.21	1.27	1.81	1.92
AFA	0.10	0.51	1.06	1.82
AAA	0.21	0.83	1.00	1.68

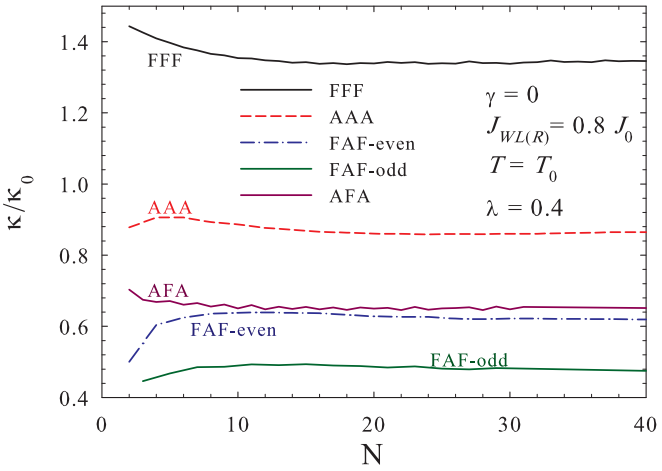

FIG. 7. Magnon thermal conductances of FFF, AAA, FAF, and AFA versus the number of moments in the center part when γ is taken as zero. Here, $J_{WL(R)} = 0.8J_0$, $J_{L(R,W)} = J_0$, $\lambda = 0.4$, and $T = T_0$.

materials is on the order of ten times the electron mass [49], at the temperature $T = T_0 \approx 120$ K, the value of the thermal magnon wavelength ($=h/\sqrt{2\pi m^* k_B T}$) is on the order of nanometers. It seems that for large N, the thermodynamic limit occurs and the magnon thermal conductance tends to a constant. Indeed, due to the short-range nature of magnon-phonon interaction that we considered here, the increase in system length moves the conductance rapidly to the thermodynamic limit. The case of FAF has two different curves for even and odd N and consequently two thermodynamic limits. In this configuration, adding a magnetic moment in the antiferromagnetic parts creates a symmetric (if N becomes even) or asymmetric (if N becomes odd) structure. The results show that the symmetric one has higher thermal conductance with respect to the asymmetric one.

IV. CONCLUSION

In this paper, we studied the magnonic transport properties of a magnetic chain in the presence of the magnon-phonon interaction. The chain is connected to two semi-infinite magnon rigid leads. We considered four configurations of FFF, FAF, AFA, and AAA built by ferromagnetic (F) and antiferromagnetic structures in the rules of center wire and leads. The magnon transmission coefficient, which depends on phonon modes, is calculated by means of the equilibrium Green's function technique. Then, the thermal average of the magnon transmission coefficient is obtained within the canonical ensemble at a certain temperature. Also, the magnon thermal conductance is computed using this quantity after taking the average of the phonon modes. Two types of local ($\gamma \neq 0$) and nonlocal ($\lambda \neq 0$) terms are investigated for magnon-phonon interaction. The local one causes a dissipative coefficient for magnons and the nonlocal term changes the coupling coefficient between the neighboring moments.

The results show that generally the magnon conductance decreases in the presence of magnon-phonon interaction, and the greatest effect is experienced by antiferromagnetic

nanowires. In more detailed consideration, we found that when the incoming magnon frequency lies in the range of magnon quasifrequencies of the center wire, the magnon conductance decreases, while in the tunneling region it is improved. By analyzing the fitting data on the middle peaks of the magnon transmission curve, we find that the transmission coefficient exponentially decays by the dissipative coefficient. The fitting procedure shows that it has decreasing behavior as a Hill function in terms of nonlocal magnon-phonon interaction strength. The same scenario is also established for magnon thermal conductance at a certain temperature. The major result is obtaining a relation between finding the microscopic quantity of nonlocal magnon-phonon interaction strength and the observable macroscopic quantity of magnon thermal conductance. Finally, the relationship between magnon thermal conductance and its scattering length is presented. In addition, it is understood that at the same taking values, the nonlocal magnon-phonon interaction has more influence on the transport properties of magnon with respect to the local one.

[1] N. Hlubek, P. Ribeiro, R. Saint-Martin, A. Revcolevschi, G. Roth, G. Behr, B. Büchner, and C. Hess, Phys. Rev. B **81**, 020405(R) (2010).

[2] A. Brumfield and J. T. Haraldsen, Crystals **9**, 93 (2019).

[3] T. Kawamata, N. Takahashi, T. Adachi, T. Noji, K. Kudo, N. Kobayashi, and Y. Koike, J. Phys. Soc. Jpn. **77**, 034607 (2008).

[4] Q. R. Zhao, M. J. Sun, Z. X. Liu, and J. Wang, Phys. Rev. B **105**, 094401 (2022).

[5] T. Kawamata, H. Sudo, Y. Matsuoka, K. Naruse, M. Ohno, T. Sasaki, and Y. Koike, J. Phys.: Conf. Ser. **568**, 042013 (2014).

[6] A. V. Sologubenko, K. Giannò, H. R. Ott, A. Vietkine, and A. Revcolevschi, Phys. Rev. B **64**, 054412 (2001).

[7] A. V. Chumak, V. I. Vasyuchka, A. A. Serga, and B. Hillebrands, Nat. Phys. **11**, 453 (2015).

[8] A. V. Sologubenko, E. Felder, K. Giannò, H. R. Ott, A. Vietkine, and A. Revcolevschi, Phys. Rev. B **62**, R6108 (2000).

[9] Z. Musavi, H. Rabani, and M. Mardaani, J. Magn. Magn. Mater. **484**, 367 (2019).

[10] Z. Musavi, H. Rabani, and M. Mardaani, J. Magn. Magn. Mater. **502**, 166494 (2020).

[11] C. Hess, B. Büchner, U. Ammerahl, L. Colonescu, F. Heidrich-Meisner, W. Brenig, and A. Revcolevschi, Phys. Rev. Lett. **90**, 197002 (2003).

[12] D. Ghader and A. Khater, Sci. Rep. **9**, 15220 (2019).

[13] A. T. Pierce, Y. Xie, S. H. Lee, P. R. Forrester, D. S. Wei, K. Watanabe, T. Taniguchi, B. I. Halperin, and A. Yacoby, Nat. Phys. **18**, 37 (2022).

[14] M. Saito, R. Takagishi, N. Kurita, M. Watanabe, H. Tanaka, R. Nomura, Y. Fukumoto, K. Ikeuchi, and R. Kajimoto, Phys. Rev. B **105**, 064424 (2022).

[15] K. Kudo, M. Yamazaki, T. Kawamata, T. Noji, Y. Koike, T. Nishizaki, N. Kobayashi, and H. Tanaka, J. Phys. Soc. Jpn. **73**, 2358 (2004).

[16] V. R. Shaginyan, A. Z. Msezane, M. Y. Amusia, J. W. Clark, G. S. Japaridze, V. A. Stephanovich, and Y. S. Leevik, Condens. Matter **4**, 75 (2019).

[17] T. Kawamata, N. Kaneko, M. Uesaka, M. Sato, and Y. Koike, J. Phys.: Conf. Ser. **200**, 022023 (2010).

[18] M. Ohno, T. Kawamata, M. Akoshima, and Y. Koike, J. Phys. Soc. Jpn. **88**, 064708 (2019).

[19] A. Suresh, U. Bajpai, and B. K. Nikolic, Phys. Rev. B **101**, 214412 (2020).

[20] S. Ghosh, F. Freimuth, O. Gomonay, S. Blügel, and Y. Mokrousov, Commun. Phys. **5**, 69 (2022).

[21] X. Chen, J. Kim, Q. Jia, S. E. Sullivan, Y. Xu, K. Jarvis, J. Zhou, and L. Shi, Adv. Funct. Mater. **30**, 2001637 (2020).

[22] L. Y. Nie, L. Wang, L. H. Zhao, and K. Q. Chen, Phys. Lett. A **364**, 343 (2007).

[23] D. T. Morelli, J. P. Heremans, and G. A. Slack, Phys. Rev. B **66**, 195304 (2002).

[24] H. Fröhlich and W. Heitler, Proc. R. Soc. A **155**, 640 (1936).

[25] D. J. Sanders and D. Walton, Phys. Rev. B **15**, 1489 (1977).

[26] A. Hoffmann, J. Magn. Magn. Mater. **539**, 168391 (2021).

[27] A. Hoffmann, IEEE Trans. Magn. **49**, 5172 (2013).

[28] S. M. Rezende, R. L. Rodríguez-Suárez, R. O. Cunha, A. R. Rodrigues, F. L. A. Machado, G. A. Fonseca Guerra, J. C. Lopez Ortiz, and A. Azevedo, Phys. Rev. B **89**, 014416 (2014).

[29] K. Nakata, J. Klinovaja, and D. Loss, Phys. Rev. B **95**, 125429 (2017).

[30] H. L. Che, J. Shi, J. C. Wu, X. Rao, X. G. Liu, X. Zhao, and X. F. Sun, AIP Adv. **8**, 055811 (2018).

[31] C. Cazorla and R. Rurali, Phys. Rev. B **105**, 104401 (2022).

[32] K. Vandaele, S. J. Watzman, B. Flebus, A. Prakash, Y. Zheng, S. R. Boona, and J. P. Heremans, Mater. Today Phys. **1**, 39 (2017).

[33] Z. N. XianYu and A. Du, J. Appl. Phys. **124**, 184304 (2018).

[34] K. Nakata and Y. Ohnuma, Phys. Rev. B **104**, 064408 (2021).

[35] C. Hess, P. Ribeiro, B. Büchner, H. ElHaes, G. Roth, U. Ammerahl, and A. Revcolevschi, Phys. Rev. B **73**, 104407 (2006).

[36] A. Sud, C. W. Zollitsch, A. Kamimaki, T. Dion, S. Khan, S. Iihama, S. Mizukami, and H. Kurebayashi, Phys. Rev. B **102**, 100403(R) (2020).

[37] C. Hess, Eur. Phys. J.: Spec. Top. **151**, 73 (2007).

[38] S. Datta, *Electronic Transport in Mesoscopic Systems* (Cambridge University Press, Cambridge, 1998).

[39] B. Raquet, M. Viret, E. Sondergard, O. Cespedes, and R. Mamy, Phys. Rev. B **66**, 024433 (2002).

[40] A. V. Savin, G. P. Tsironis, and X. Zotos, Phys. Rev. B **72**, 140402(R) (2005).

[41] A. L. Chernyshev and A. V. Rozhkov, Phys. Rev. B **72**, 104423 (2005).

[42] C. Kittel, *Introduction to Solid State Physics* (Wiley, New York, 2005).

[43] F. Bloch, Z. Phys. **61**, 206 (1930).

[44] J. V. Kranendonk and J. H. V. Vleck, Rev. Mod. Phys. **30**, 1 (1958).

[45] A. Kwaśniowski and J. Adamowski, J. Phys.: Condens. Matter **20**, 215208 (2008).

[46] M. M. Bezerra-Neto, M. S. Ribeiro, B. Sanyal, A. Bergman,

R. B. Muniz, O. Eriksson, and A. B. Klautau, Sci. Rep. **3**, 3054 (2013).
[47] M. Zare, F. Parhizgar, and R. Asgari, J. Magn. Magn. Mater. **456**, 307 (2018).
[48] G. Grosso and G. P. Parravicini, *Solid State Physics*, 2nd ed. (Academic Press, New York, 2013).
[49] J. R. Hook and H. E. Hall, *Solid State Physics*, 2nd ed. (Wiley, New York, 1995).
[50] M. Mardaani, H. Rabani, E. Esmaili, and A. Shariati, J. Appl. Phys. **118**, 054306 (2015).
[51] M. Mardaani and H. Rabani, Phys. Status Solidi B **251**, 1001 (2014).
[52] K. Wang, X. Xu, Y. Cheng, M. Zhang, J. S. Wang, H. Wang, and G. Zhang, Appl. Phys. Lett. **118**, 023102 (2021).
[53] S. Datta, *Quantum Transport: Atom to Transistor* (Cambridge University Press, Cambridge, 2005).
[54] E. Esmaili, M. Mardaani, and H. Rabani, Superlattices Microstruct. **113**, 110 (2018).
[55] M. Mardaani and H. Rabani, J. Magn. Magn. Mater. **331**, 28 (2013).